Femtosecond Light Transmission and Subradiant Damping in Plasmonic Crystals

C. Ropers,[1] D. J. Park,[2] G. Stibenz,[1] G. Steinmeyer,[1] J. Kim,[3] D. S. Kim,[2,*] and C. Lienau[1,†]

[1]*Max-Born-Institut für Nichtlineare Optik und Kurzzeitspektroskopie, D-12489 Berlin, Germany*

[2]*School of Physics, Seoul National University, Seoul 151-742, Korea*

[3]*Korea Research Institute of Standards and Science, Yusung, Taejon 305-600, Korea*

(Received 20 October 2004; published 21 March 2005)

We report the first observation of subradiance in plasmonic nanocrystals. Amplitude- and phase-resolved ultrafast transmission experiments directly reveal the coherent coupling between surface plasmon polaritons (SPPs) induced by periodic variations in the dielectric function. This interaction results in the formation of plasmonic band gaps and coupled SPP eigenmodes with different symmetries, as directly shown by near-field imaging. In antisymmetric modes, radiative SPP damping is strongly suppressed, increasing the SPP lifetime from 30 fs to more than 200 fs. The findings are analyzed within a coupled resonance model.

DOI: 10.1103/PhysRevLett.94.113901 PACS numbers: 42.70.Qs, 07.79.Fc, 42.25.–p, 73.20.Mf

Surface-bound electromagnetic waves on metals, so-called surface plasmon polaritons (SPPs), will play a key role in novel photonic structures, promising an unprecedented amount of microscopic light control [1–4]. Nanohole and nanoslit arrays in metal films are a particularly important model system for SPP nano-optics. In such plasmonic crystals, recent time-resolved experiments have demonstrated a strong SPP-coupling to far-field radiation, limiting SPP lifetimes to few tens of femtoseconds [5,6]. This poses a constraint on using these structures in novel elements such as plasmonic resonators or nanowaveguides. The question arises how to control radiative SPP damping in order to overcome these constraints.

In general, radiative decay phenomena can be strongly modified by coherent couplings between the relevant optical excitations. For two resonant systems, e.g., two atoms separated by less than one wavelength, the radiative coupling leads to the formation of collective states and cooperative effects in their radiative decay, namely, superradiance and subradiance [7]. Specifically, subradiance reflects the suppression of radiative damping of the collective state with antisymmetric character of the wave function. These phenomena are of great interest as they play a dominant role in the optical properties of many dense, microscopic systems, e.g., trapped ions [8], Bose-Einstein condensates [9], molecular aggregates [10], or coupled semiconductor quantum dots [11] and wells [12].

In plasmonic crystals, both the coherent coupling between polaritonic excitations and their coupling to the radiation field is induced by periodic variations of the dielectric function [13]. Whereas the resulting band gap formation has received much attention, there are only a few studies of coupling-induced phenomena in the radiative damping of polariton modes [14,15].

In this Letter, we report the first experimental evidence for subradiant damping in plasmonic crystals. Ultrafast pulse transmission experiments demonstrate a more than sevenfold enhancement of SPP lifetimes induced by the coherent coupling among SPP modes. Near-field optical measurements show directly that the formation of antisymmetric modes is the origin of the radiative damping suppression.

We investigate 150 nm thick gold films deposited on 100 μm sapphire substrates and perforated with linear arrays of 50 nm wide slits with periods a_0 of 650 and 750 nm. Such narrow slits were chosen to minimize radiative damping [5]. The samples are illuminated with weakly collimated 11 fs light pulses from a Ti:sapphire oscillator centered at a wavelength of 800 nm, linearly (TM) polarized perpendicular to the slits. The incident electric field is characterized by spectral phase interferometry for direct electric field reconstruction [16]. Interferometrically heterodyning the incident and the transmitted pulses, we determine the transmission function via spectral interferometry [17]. With the amplitude and phase of both, the incident pulse and the transmission function of the nanoslit array, we compute the electric field at the output of the array and determine its temporal structure via a Fourier transform. In further experiments, SPP mode profiles are spatially and spectrally resolved with a near-field microscope in transmission geometry for TM-polarized excitation [5,18].

In such nanoslit arrays, SPPs at both the air-metal (AM) and the sapphire-metal (SM) interfaces of the metal film can be resonantly excited by grating coupling, transferring momentum $\Delta k = p \cdot G = p \cdot 2\pi/a_0$, with an integer p, to the incident photons [4]. Excitations at the two interfaces are coupled via the nanoslit wave guide channel, and two different pathways can contribute to the transmission through these plasmonic crystals [19,20]: nonresonant direct transmission through the nanoslit wave guide and resonant excitation and subsequent reemission of SPPs. Time-resolved measurements of the electric field of 11 fs incident laser pulses and of the pulses transmitted through a nanoslit array with a period of 650 nm [Fig. 1(a)] give direct evidence for this picture. The time structure of the

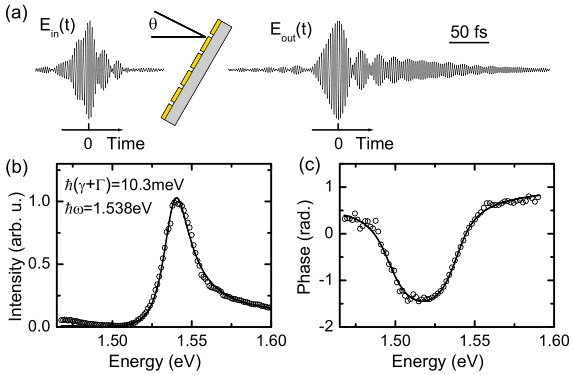

FIG. 1 (color online). (a) Time structure of the electric field $E_{\mathrm{in}}(t)$ of the incident 11 fs pulses and of the pulses $E_{\mathrm{out}}(t)$ transmitted through a nanoslit array with $a_0 = 650$ nm at an angle θ of 8°. (b) Representative transmission spectrum $T(\omega) = |E_{\mathrm{out}}(\omega)/E_{\mathrm{in}}(\omega)|^2$ and (c) spectral phase $\varphi(\omega) = \arg[E_{\mathrm{out}}(\omega)/E_{\mathrm{in}}(\omega)]$ (open circles) near the SM[− 2] resonance. Solid lines: Fit to Eq. (1) with parameters indicated in (b).

transmitted field reveals these two distinct components: the initial peak around time zero mainly reflects the nonresonant transmission, whereas the long-lived signal persisting beyond 30 fs is due to resonant SPP reemission.

In the spectral domain, the interference between these two channels gives rise to asymmetric Fano-like line shapes in the far-field transmission spectra $T(\omega) = |t(\omega)|^2$ with

$$t(\omega) = a_{\mathrm{nr}} + \sum_j \frac{b_j \Gamma_j e^{i\phi_j}}{\omega - \omega_j + i(\gamma_j + \Gamma_j)}. \qquad (1)$$

Here a_{nr} is a slowly varying amplitude and b_j and ϕ_j characterize amplitude and phase of the SPP resonances. The real frequencies ω_j correspond to SPP resonances at either the AM or SM interface [21]. The resonance width contains two contributions: a nonradiative damping γ_j due to absorption in the metal, and the radiative damping Γ_j of the SPP modes, which is in most cases dominant [5]. Figs. 1(b) and 1(c) show the intensity $T(\omega)$ and phase $\varphi(\omega) = \arg[t(\omega)]$ of the transmission function at a sapphire-metal resonance (open circles). A simultaneous fit to Eq. (1) including only a single resonance (solid lines) at $\hbar\omega = 1.538$ eV indicates quite good agreement with experiment. It shows, in particular, that for a single SPP resonance the total linewidth $\hbar(\gamma + \Gamma) = 10.3$ meV is much larger than the intrinsic Ohmic losses on a planar gold film of about $\hbar\gamma = 2.5$ meV. Thus, the resonance is predominantly radiatively broadened and the SPP lifetime $T_1 = 1/2(\gamma + \Gamma)$ is about 32 fs.

This quantitative understanding of the line shape function is the key to the analysis of coherent SPP couplings. To investigate band gap formation and radiative decay phenomena, we have performed angle-resolved spectral interferometry on an array with 650 nm period, chosen for optimum overlap of the SM[+ 1, −2] resonances with the laser spectrum. In such experiments, the in-plane momentum $k_x = \frac{\omega}{c}\sin\theta + p \cdot 2\pi/a_0$ and thus the resonance energy of the excited SPP mode is continuously varied by changing the angle of incidence θ, allowing for a mapping of the SPP band structure [4,21]. Figure 2 shows transmission spectra $T(\omega, \theta)$ and $\varphi(\omega, \theta)$ between 700 and 900 nm. Resonances connected to SPPs on both sides of the gold film, namely, AM[$p = \pm 1$] and SM[$p = \pm 1, 2$], are clearly resolved. At all angles, the spectra and the phase curves are consistently modeled by Eq. (1), taking the relevant SPP resonances into account.

This analysis allows to precisely measure the SPP band structure $\omega_j(\theta)$. The resulting frequencies near the crossing of SM[+1] and SM[−2] around 36° are plotted as open circles in Fig. 2(a). One observes a clear anticrossing of the SPP bands with a band gap energy of about 72 meV.

Near the crossing, there are pronounced variations of the intensities and linewidths of the two modes. In particular, as θ approaches the crossing, the lower energy mode becomes narrower until the transmission intensity begins to decrease. This reduction in linewidth reflects the suppression of radiative SPP damping due to the coupling of SM[+1] and SM[−2] resonances.

Both subradiant SPP decay and band gap formation are expected to be intimately connected with the formation of new coupled SPP eigenmodes of different spatial symmetry [7,22,23]. To demonstrate this link, we have performed spatially and spectrally resolved near-field measurements near the crossing of two air-metal bands. We switched to an array with $a_0 = 750$ nm, redshifting all resonances by about 100 nm and providing better overlap of the AM[+1]/AM[−1] crossing with the laser spectrum. Here the far-field transmission spectra near normal incidence [Fig. 3(a)] show two asymmetric transmission peaks, a spectrally broad and intense low energy resonance at

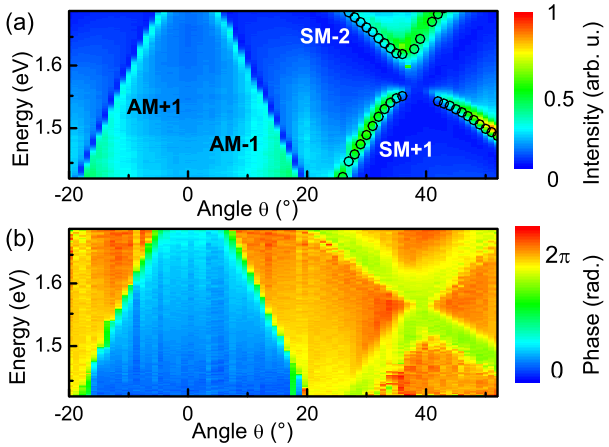

FIG. 2 (color online). Angle-resolved transmission $T(\omega, \theta)$ (a) and phase $\varphi(\omega, \theta)$ for a nanoslit array with $a_0 = 650$ nm. Open circles: SPP band structure $\omega_j(\theta)$ near the crossing of SM[+ 1] and SM[− 2] resonances, obtained by fitting to Eq. (1). A band gap of 72 meV is revealed.

1.55 eV (bright mode) and a much narrower and weaker high energy peak at 1.62 eV (dark mode). Angle-dependent far-field spectra displayed in Fig. 3(b) reveal a drastic change in linewidth of the dark mode for small incidence angles. This linewidth decrease corresponds to a sevenfold increase in SPP lifetime T_1 to more than 200 fs when θ is reduced from 1.2 to 0.5 degrees [Fig. 3(c)].

Near-field maps of the SPP field at these transmission resonances are displayed in Fig. 4(a). Here, the sample was illuminated from the substrate side with slightly focused (opening angle $\Delta\theta = 2\,^\circ$) monochromatic light from a Ti:sapphire laser at $\theta \simeq 0\,^\circ$. The intensity of the transverse field component $I(x)$ was probed through a fiber tip with a 50 nm thick Al coating and a 100 nm aperture [5,18]. In the energy region of the bright resonance, $I(x)$ shows maxima at the slits and weaker maxima in the center between slits [Fig. 4(c)]. As the energy is tuned towards the dark mode, $I(x)$ gradually shifts. At the dark mode energy, $I(x)$ shows almost negligible intensity at the slits and two strong maxima at $\pm a_0/4$ [Fig. 4(b)].

We now discuss how this difference in spatial mode profiles is connected to the radiative damping. We first look at the SPP eigenmode solutions of Maxwell's equations for our nanoslit arrays. For vanishing slit width these are simply evanescent plane SPP modes $|j\rangle$ with frequencies ω_j, a nonradiative damping γ_j, and electric field profiles $\mathbf{E}_j(\mathbf{r})$. For simplicity, we consider only two nearly resonant modes $|1\rangle$ and $|2\rangle$, e.g., the AM[$\pm$ 1] modes in case of Figs. 3 and 4. The change in the dielectric function induced by the nanoslits locally changes the electromagnetic energy density and thus leads to frequency shifts V_{11} and V_{22} and, most importantly, to a coupling V_{12} of the two modes. To first order, the strength of these interactions can be approximated as $V_{ij} \simeq \langle i|\epsilon^2\Delta(\epsilon(\mathbf{r})^{-1})|j\rangle/\hbar$ [24], where $\Delta\epsilon(\mathbf{r})$ denotes the local perturbation of the dielectric function [25].

Moreover, the nanoslits induce a coupling of the evanescent SPP modes of the ideal interfaces to the continuum of propagating far-field modes $|m\rangle$ [20], i.e., radiative damping $\Gamma_{ij} \simeq (2\pi/\hbar)\sum_m \langle i|\epsilon^2\Delta(\epsilon(\mathbf{r})^{-1})|m\rangle \times \langle m|\epsilon^2\Delta(\epsilon(\mathbf{r})^{-1})|j\rangle$. It is essential that the presence of the slits not only leads to a damping of the individual resonances $(\Gamma_{11}, \Gamma_{22})$ but also causes a radiative coupling $(\Gamma_{12}, \Gamma_{21})$ among the SPP modes via the far-field continuum. These terms can be cast into a coupled mode matrix with eigenvalues describing the resonances of the coupled system and their radiative decay:

$$\begin{pmatrix} \omega_1 - i\gamma_1 & 0 \\ 0 & \omega_2 - i\gamma_2 \end{pmatrix} + \begin{pmatrix} V_{11} - i\Gamma_{11} & V_{12} - i\Gamma_{12} \\ V_{21} - i\Gamma_{21} & V_{22} - i\Gamma_{22} \end{pmatrix}. \tag{2}$$

The detuning $\Delta(k_x) = \omega_2(k_x) - \omega_1(k_x)$ between the two unperturbed resonances follows from the SPP dispersion relation of the unpatterned film and is continuously varied by angle tuning. For the AM[$\pm$ 1] resonance and small angles, all coupling $V \simeq V_{ij}$ and damping constants $\Gamma \simeq \Gamma_{ij}$, $\gamma \simeq \gamma_j$ are nearly identical and the frequencies of the coupled modes are given as $\omega_{+,-} = \omega_1 + \Delta/2 + V - i\Gamma \pm A/2$ with $A = \sqrt{\Delta^2 + 4(V - i\Gamma)^2}$. The resulting coupled eigenmodes are $|+,-\rangle = \pm c_1|1\rangle + c_2|2\rangle$, with coefficients $c_{1,2} = \sqrt{(A \mp \Delta)/2A}$. Using this model, optical transmission spectra can be simulated by using Eq. (1).

The coupling between these two resonances results in the opening of SPP band gaps $2\hbar V$ when the SPP modes are angle tuned into resonance [Fig. 2(a)]. This band gap formation coincides with a pronounced change of the linewidth $\Gamma_- = \gamma + \Gamma - \mathrm{Im}(A/2)$ of the newly formed antisymmetric (dark) $|-\rangle$ mode. Its radiative coupling to the far-field continuum $\Gamma_{r-} = \Gamma - \mathrm{Im}(A/2)$ decreases

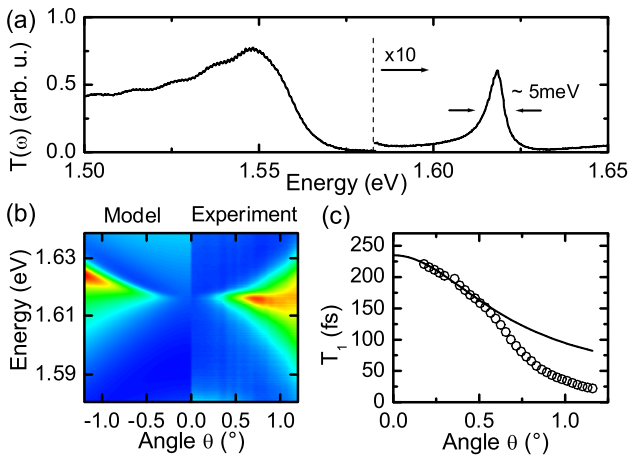

FIG. 3 (color online). (a) Transmission spectrum $T(\omega)$ through a nanoslit array with $a_0 = 750$ nm near normal incidence ($\theta \sim 0.6\,^\circ$). (b) Angle-dependent spectra in model (left) and experiment (right). (c) Experimentally determined SPP lifetime T_1 as a function of θ.

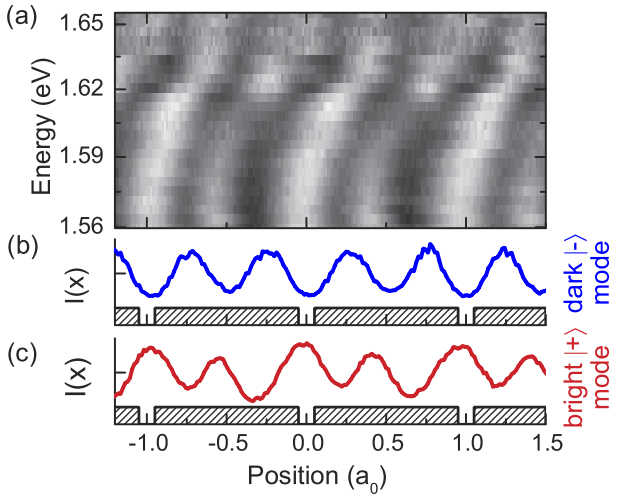

FIG. 4 (color online). (a) Spatially resolved near-field mode profiles $I(x, E)$ recorded as a function of excitation energy E by scanning perpendicular to the slits. At each energy, the data are normalized to $\int I(x)dx$. (b) $I(x)$ of the antisymmetric mode $|-\rangle$ at 1.62 eV. (c) $I(x)$ of the symmetric mode $|+\rangle$ at 1.56 eV.

continuously with decreasing detuning, and radiative damping is fully suppressed at $\Delta = 0$. Here, the linewidth of the resonance is no longer limited by radiative damping but by the intrinsic losses γ. In angle-dependent spectra [Fig. 3(b)], one thus observes a narrowing of the resonance with decreasing θ until $\Gamma_{r-} < \gamma$, followed by a decrease of the intensity of the dark mode peak which vanishes at $\Delta = 0$. The results in Fig. 3(b) and 3(c) are satisfactorily modeled by Eq. (2) when parameters $\hbar V = 35$ meV and $\hbar\Gamma = 13$ meV are assumed. The slightly stronger variation in the experimentally measured linewidth is mainly attributed to an oversimplified modelling of the nonresonant transmission continuum in Eq. (1).

The microscopic origin of this pronounced suppression of radiative damping becomes immediately apparent from the spatial near-field mode profiles in Fig. 4. The mode overlap of the symmetric $|+\rangle$ mode [Fig. 4(c)] with the nanoslit scattering centers is larger than that of the uncoupled modes $|1, 2\rangle \propto \exp(\pm iGx)$, thus increasing the radiation damping Γ_+. For the antisymmetric $|-\rangle$ mode [Fig. 4(b)], however, the maxima of $I(x) \simeq |\exp(iGx) - \exp(-iGx)|^2$ at $\pm a_0/4$ are now outside the nanoslits. The field intensity at the nanoslits is strongly reduced and the radiative damping rate Γ_{r-} becomes vanishingly small. This is in analogy to previously observed interference phenomena in the radiative damping of other, e.g., atomic or molecular, multilevel systems [8,26]. In such systems, however, the finite radiative damping of the uncoupled systems is often larger than their radiative coupling and the suppression of radiative damping is much less pronounced [8]. In the system considered here, the intrinsic damping is sufficiently weak to reach the strong radiative coupling limit ($\Gamma > \gamma$).

While the introduced phenomenological model captures the physical mechanisms underlying the observed coupling phenomena, a more refined calculation of the optical transmission spectra can be obtained from a full, scattering-matrix-based solution of Maxwell's equations [22]. Such calculations show that in one-dimensional nanoslit arrays, the coupling parameters are affected by Fabry-Perot effects and thus depend on the actual thickness of the metal film [27]. Such effects appear, because subwavelength 1D structures always support a propagating mode within the nanoslit wave guide channel, in contrast to the evanescent wave guide mode in nanohole arrays. For the geometrical parameters of our slit structures, the coupling parameters deduced from such a refined calculation are in satisfactory agreement with experiment, supporting the interpretation of our results.

In conclusion, we have studied the coherent coupling of surface plasmon polaritons in plasmonic nanocrystals using space- and time-resolved optical spectroscopy. We demonstrate that the formation of antisymmetric SPP modes gives rise to a pronounced suppression of radiative damping and leads to surprisingly long SPP lifetimes of more than 200 fs. Such a control of radiative damping by tailoring SPP mode profiles is an essential prerequisite for designing and implementing efficient nanoplasmonic devices such as wave guides or resonators, studying the physics of strong SPP localization and using SPP as flying qubits in quantum information processing.

Financial support of the work in Korea by MOST and KOSEF and that in Germany by the DFG (SFB296) is gratefully acknowledged. We thank Q-Han Park and Thomas Elsaesser for helpful discussions.

*Electronic address: denny@snu.ac.kr
†Electronic address: lienau@mbi-berlin.de

[1] W. L. Barnes *et al.*, Nature (London) **424**, 824 (2003).
[2] H. J. Lezec *et al.*, Science **297**, 820 (2002).
[3] S. A. Maier *et al.* Nat. Mater. **2**, 229 (2003).
[4] T. W. Ebbesen *et al.*, Nature (London) **391**, 667 (1998).
[5] D. S. Kim *et al.*, Phys. Rev. Lett. **91**, 143901 (2003).
[6] A. Dogariu *et al.*, Opt. Lett. **26**, 450 (2001).
[7] R. H. Dicke, Phys. Rev. **93**, 99 (1954).
[8] R. G. DeVoe and R. G. Brewer, Phys. Rev. Lett. **76**, 2049 (1996).
[9] D. Schneble *et al.*, Science **300**, 475 (2003).
[10] S. H. Lim *et al.*, Phys. Rev. Lett. **92**, 107402 (2004).
[11] Y. N. Chen, D. S. Chuu, and T. Brandes, Phys. Rev. Lett. **90**, 166802 (2003).
[12] M. Hübner *et al.*, Phys. Rev. Lett. **76**, 4199 (1996).
[13] J. D. Joannopoulos, R. D. Meade, and J. N. Winn, *Photonic Crystals* (Princeton University, Princeton, NJ, 1995).
[14] A. Christ *et al.*, Phys. Rev. Lett. **91**, 183901 (2003).
[15] T. Zentgraf *et al.*, Phys. Rev. Lett. **93**, 243901 (2004).
[16] C. Iaconis and I. A. Walmsley, Opt. Lett. **23**, 792 (1998).
[17] F. Reynaud, F. Salin, and A. Barthelemy, Opt. Lett. **14**, 275 (1989).
[18] S. C. Hohng *et al.*, Appl. Phys. Lett. **81**, 3239 (2002).
[19] M. Sarrazin, J.-P. Vigneron, and J.-M. Vigoureux, Phys. Rev. B **67**, 085415 (2003).
[20] C. Genet, M. P. van Exter, and J. P. Woerdman, Opt. Commun. **225**, 331 (2003).
[21] H. F. Ghaemi *et al.*, Phys. Rev. B **58**, 6779 (1998).
[22] S. G. Tikhodeev *et al.*, Phys. Rev. B **66**, 045102 (2002).
[23] P. Paddon and J. F. Young, Phys. Rev. B **61**, 2090 (2000).
[24] S. G. Johnson *et al.*, Phys. Rev. E **65**, 066611 (2002).
[25] Because of the field discontinuities at the slits some care is needed in using perturbation expressions [24]. We find, however, that the values of $\hbar|V| \simeq 30$ meV at the AM[± 1] resonance for 50 nm slits and $a_0 = 750$ nm agree quite well with a nonperturbative solution.
[26] U. Akram, Z. Ficek, and S. Swain, Phys. Rev. A **62**, 013413 (2000), and references therein.
[27] J. A. Porto, F. J. Garcia-Vidal, and J. B. Pendry, Phys. Rev. Lett. **83**, 2845 (1999).